Dynamics of a Cholera Transmission Model with Immunological Threshold and Natural Phage Control in Reservoir

Jude D. Kong · William Davis · Hao Wang

Abstract Cholera remains epidemic and endemic in the world, causing thousands of deaths annually in locations lacking adequate sanitation and water infrastructure. Yet, its dynamics are still not fully understood. In this paper, we simplify and improve Jensen et al.'s model (PNAS 103:4652–4657, 2006) by incorporating a Minimum Infection Dose (MID) into the incidence term. We perform local stability analysis and provide bifurcation diagrams of the bacterial carrying capacity with or without shedding. Choosing parameters such that the endemic or epidemic equilibrium is unstable (as it is the case in reality), we observe numerically that for the bacterial carrying capacity (K) less than the MID (c), oscillating trajectories exist only in the microbial scale, whereas for $K > c$, they exist in both the microbial and population scales. In both cases, increasing pathogen shed rate ξ increases the amplitude of the trajectories and the period of the trajectories for those that are periodic. Our findings highlight the importance of the relationship among the shedding rates, K, MID, the maximum bacterial growth rate (r) and the features of the disease outbreak. In addition, we identified a region in the parameter space of our model that leads to chaotic behaviour. This could be used to explain the irregularity in the seasonal patterns of outbreaks amongst different countries, especially if the positive relationship between bacterial proliferation and temperature is considered.

Keywords Cholera · Indirect transmission · Immunological threshold · Phage · Stability analysis

J. D. Kong · W. Davis · H. Wang (✉)
Department of Mathematical and Statistical Sciences, University of Alberta, Edmonton, AB T6G 2G1, Canada
e-mail: hao8@ualberta.ca

J. D. Kong
e-mail: jdkong@ualberta.ca

1 Introduction

Cholera is a disease of the intestinal tract, which causes severe diarrhoea, leading to dehydration which if left untreated can cause death. It is caused by the bacteria *Vibrio cholerae* and is treatable if caught within 1–2 days of symptoms first appearing. In places with adequate health care and access to antibiotics, cholera is not much of a problem. However, in countries where such health services are lacking in a permanent sense or because of natural disasters reducing their availability, cholera outbreaks are still a concern. Dhaka, the capital of Bangladesh, for example, has two outbreaks of cholera per year (Islam et al. 1994) that occur with the changes in seasons and the amount of rainfall, both of which affect the quality of the water supply.

Despite being studied for more than 100 years by the likes of English physician John Snow in the mid 1800s (Snow 1985) and many others, the transmission dynamics of the disease are not fully understood. The role of blue-green algae, which is present in the water supplies of countries like Bangladesh, has been suggested by some (Islam et al. 1994) as a reservoir that the bacteria can exist in during inter-epidemic times. However, this does not explain its natural cycles completely. One problem in understanding the dynamics is that *V. cholerae* is always found in lower levels than predicted, leading to possible explanations that *V. cholerae* can revert from a culturable form to a viable but not culturable form within the human body (Colwell et al. 1996). Experiments show that *V. cholerae* becomes many times more infectious for a short period of time once it has passed through the human digestive tract (Hartley et al. 2006). A more complete understanding of how exactly *V. cholerae* is transmitted through populations will certainly help improve the control of outbreaks in the future for regions where it is an issue.

The contributions from mathematical modelling indicate that mathematical modelling is a promising way to look into the nature of the cholera dynamics. Many mathematical differential equation models have been proposed. Among these, the main ones that make use of ordinary differential equations are those built upon the Cappasso–Fontona model (1979) and the Codeço model (2001). Codeço model (2001) is considered to be the first modern cholera model. The author divided the human population into three compartments; Susceptible, Infected and Recovered compartments. The recovered compartment was not started explicitly, as the population was assumed to be constant. The author equally assumed that there is no disease-induced mortality. He represented the aquatic reservoir very simply with a linear growth term and linear shedding contribution. This was because the ecological dynamics of *V. cholerae* were not well understood at the time (they are still not completely understood). The oscillations in this system die out over time; so in order to simulate the periodic behaviour of outbreaks observed in some endemic areas, periodic contact rates, shedding rates and net growth rates of bacteria were also included. Hartley et al. (2006) incorporated a hyperinfectious route of transmission to the Codeço model, and Joh et al. (2009), Tian et al. (2011), Jensen et al. (2006) and Mukanvire et al. (2011) have further built on and branched off from these models.

Aimed at taking into account the role of bacteriophage which has been suggested by experimentalists as important, Jensen et al. (2006) modified the Codeço model to include a phage compartment P, and dividing infectives into bacteria and phage

infected, and phage-infected individuals. Bacteria are assumed to experience logistic growth with carrying capacity, and predation by phage occurs via a Holling I response. The infection term is a Holling III functional response. The sigmoidal shape is intended to capture the low infectivity of low levels of bacteria, but there are still infections at very small levels which could overestimate the number of infections in the long run. The focus of this model was to determine the ability of phage to end outbreaks or indirectly cause outbreaks by being reduced in number. Both of these abilities were demonstrated in the analysis. However, they did not examine the role, or existence, of limit cycles caused by the predator–prey-like relationship of phage and bacteria, which is something we will pay attention to in the presence and absence of human shedding. In particular, we will show that cycles observed in the human population (macro scale) are caused by cycles in the microscale of bacteria and bacteriophage as has been suggested by Faruque et al. (2005) and others. Jensen et al. (2006) also failed to take into account the fact that bacteria have to enter the human body in higher concentrations to overwhelm the natural immune response (Murphy et al. 2007) (existence of a minimum infection dose (MID) for bacteria), something that was first considered in modelling by Joh et al. (2009). We improve this model by incorporating a MID into the incidence term. This infection term is a piecewise continuous function which is zero below the minimum infectious dose (MID) threshold and a Holling II response curve above the threshold. Similar to Jensen et al. (2006), we also allow bacteria to exist naturally under logistic growth. With these adjustments and a few others made to the model, we determine the invariant domain, carry out local stability analysis and locate limit cycles, with or without human shedding, and show numerically that by choosing parameters such that the endemic or epidemic equilibrium is unstable (as it is the case in reality), for the bacteria carrying capacity (K) less than the MID (c), oscillating trajectories exist only in the microbial scale, whereas for $K > c$, they exist in both the microbial and population scales, and that in both cases, increasing pathogen shed rate ξ increases the amplitude of the trajectories and the period of the trajectories for those that are periodic. Further, in this paper, we demonstrate the existence of a chaotic region in the parameter space, which could account for the different natures of outbreaks observed around the world.

2 Model Formulation

Bacteria and bacteriophage exist in a predator–prey relationship. We capture this interaction using a Holling II predation term $\gamma \frac{B}{K_1+B} P$, where γ is the maximum predation rate; B and P represent bacteria and phage densities, respectively; and K_1 is the half-saturation constant of predation (the bacterial level at which predation occurs at half of the maximum rate). We assume that the bacterial population experiences logistic growth in the absence of predation and human influence, with carrying capacity K and maximum growth rate r. As in Jensen et al.'s model (2006) and Codeço's model (2001), the human population is assumed to be constant, and this is assumed to be no disease-induced mortality. The lack of death due to infection as was the case in Dhaka during the 2004 outbreak , where all severe cases were treated (see Jensen et al. 2006 and reference therein), almost all endemic/epidemic regions nowadays have

hospitals that provide the right treatment. No death is inevitable with cholera if the right treatment is provided. This motivates the following model, which assumes no infection-derived immunity for simplicity:

$$
\begin{aligned}
\frac{dS}{dt} &= -\alpha(B)S + \mu I, \\
\frac{dI}{dt} &= \alpha(B)S - \mu I, \\
\frac{dB}{dt} &= rB\left(1 - \frac{B}{K}\right) - \gamma \frac{B}{K_1 + B}P + \xi I, \\
\frac{dP}{dt} &= \beta\gamma \frac{B}{K_1 + B}P - \delta P + \phi \xi I.
\end{aligned}
\tag{1}
$$

The incidence term we use is $\alpha(B)S$ where $\alpha(B)$ is the bacterial density-dependent component. The 'indirect' part of the incidence term $\alpha(B)$ is defined by

$$
\alpha(B) = \begin{cases} 0, & B < c; \\ \frac{a(B-c)}{(B-c)+H}, & B \geq c. \end{cases}
$$

Unlike in larger scale predator–prey dynamics, where β would be a measure of the conversion rate of prey into predators, often less than unity, β here represents a 'burst size', as each infected bacterial cell will give rise to many new phage cells. Human contamination of the water supply through infected faeces contributes to both bacteria and phage levels and is called 'shedding'. Bacteria and phage shedding rates need not be the same so the rate for bacteria is ξ and for phage, it is $\phi\xi$ where ϕ is some constant. In the absence of predators and humans, bacteria will exist at their carrying capacity K. We assume that phage and bacteria can live naturally without human interference, as in inter-epidemic times, and so it is assumed that $\beta\gamma > \delta$. If this is not so, phage would die out in the absence of human shedding. This maximum predation rate γ is difficult to measure, and for numerical solutions, it is chosen to satisfy this inequality. The half-saturation constant for the predation term, K_1, was also estimated, and was assumed to be less than the natural carrying capacity K so that predation does not always occur near the maximal rate. For numerical simulations, parameters are taken from the literature, and the ranges are given in Table 1.

3 Forward Invariance

We would like to define a forwardly invariant set in which solutions of (1) will be bounded. From the first two equations of (1), we see that $\dot{S}(S = 0) = \mu I$ but as $S + I = N$, we can write $\dot{S}(S = 0) = \mu N > 0$. Thus $S(t) > 0$ for $t > 0$. Even though there is no birth or death in this system, if the entire population were to be infected, there would be people recovering and moving back into the susceptible category.

Table 1 Parameter values expanded from Jensen et al. (2006) and Cash et al. (1974)

Parameter	Values	Description	Units
r	0.3–14.3	Maximum per capita pathogen growth efficiency	Day^{-1}
K	10^5–10^7	Pathogen carrying capacity	Cell liter^{-1}
H	10^6–10^8	Half-saturation pathogen density	Cell liter^{-1}
a	0.1	Maximum rate of infection	Day^{-1}
ξ	0–100	Pathogen shed rate	Cell liter^{-1} day^{-1}
μ	0.1	Human recovery rate	Day^{-1}
N	10^6	Total Population	Persons
c	10^5–10^7	MID	Cell liter^{-1}
β	80–100	Phage burst size	Virions day^{-1}
γ	0–0.025	Maximum per capita phage absorption rate	Cell virion^{-1} Day^{-1}
δ	0.5-7.9	Phage death rate	Virions day^{-1}
ϕ	10^{-6}–1	Mean phage shed rate	Virions cell^{-1}
K_1	$< K$	Half-saturation bacteria predation density	Cell liter^{-1}

Similarly, $\dot{I}(I = 0) = \alpha(B)S \geq 0$ as we just saw that $S(t) > 0$ for $t > 0$ and $\alpha(B) \geq 0$ by definition. As $S > 0$ and $I \geq 0$ then as there are only two compartments for humans, $S \leq N$ and $I < N$.

The BP system is more complicated as for upper bounds, but note that $\dot{B}(B = 0) = \xi I$ thus $B(t) \geq 0$. We have that $\dot{B} < rB\left(1 - \frac{B}{K}\right) + \xi N$ and so we can define

$$B_{\max} = \frac{rK + K\sqrt{r^2 + \frac{4r}{K}\xi N}}{2r},$$

where if $B(0) \in [0, B_{\max})$ then $B(t) \in [0, B_{\max})$ for $t \geq 0$. Finally, consider $\dot{P}(P = 0) = \phi\xi I \geq 0$ and so $P(t) \geq 0$ for all $t > 0$. The upper bound of $P(t)$ requires the following lemma.

Lemma 1 *Define positive constants u and v such that* $\frac{((r+u)\beta)^2 K}{4r\beta} < v$. *Then, for all values of B, the following is true:*

$$0 < \frac{r}{K}\beta B^2 - ((r + u)\beta)B + v.$$

We can now show that B and P are bounded above, although it was already demonstrated that B is bounded. Consider

$$\frac{\mathrm{d}}{\mathrm{d}t}(\beta B + P) < r\beta B - \frac{r}{K}B^2\beta - \delta P + (\beta + \phi)\xi N.$$

By invoking Lemma 1, we see that

$$\frac{d}{dt}(\beta B + P) < -U(\beta B + P) + (\beta + \phi)\xi N + v,$$

where $U := \min\{u, \delta\}$, which implies that $\beta B + P$ is bounded. Defining $V := (\beta + \phi)\xi N + v$, we can write

$$\limsup_{t \to \infty} \beta B(t) + P(t) \leq \frac{U}{V} \quad \text{or} \quad \beta B(t) + P(t) \leq \max\left\{\beta B(0) + P(0), \frac{U}{V}\right\}.$$

We summarize the above results with a proposition.

Proposition 1 (Feasible Region) *The set*

$$\Gamma = \{S, I, B, P \geq 0 : S + I = N, \beta B(t) + P(t) \leq \frac{U}{V}, B < B_{\max}\}$$

defines a forwardly invariant region of system (1), *where* $V := (\beta + \phi)\xi N + v$ *and* $U := \min\{u, \delta\}$, *with* $u, v > 0$ *satisfying* $\frac{((r+u)\beta)^2 K}{4r\beta} < v$.

4 Existence and Stability of Equilibria with no Shedding

4.1 Existence of Equilibria

In countries with modern sanitational infrastructure, human contamination of the water supply (shedding) is very low; in the ideal case, shedding is completely absent. We can determine the number and stability of steady states of (1) without shedding by substituting $\xi = 0$ and further noting that as $S = N - I$ the first equation is not necessary, leaving us with the following:

$$\frac{dI}{dt} = \alpha(B)(N - I) - \mu I,$$
$$\frac{dB}{dt} = rB\left(1 - \frac{B}{K}\right) - \gamma \frac{B}{K_1 + B}P, \quad (2)$$
$$\frac{dP}{dt} = \beta\gamma \frac{B}{K_1 + B}P - \delta P.$$

If the bacteria level is below the minimum infectious dose, then $\alpha(B) = 0$. The first equation of (2) implies that $I^* = 0$ in this case, and so $S^* = N$ as well. The second and third equations of (2) at steady state become

$$0 = rB\left(1 - \frac{B}{K}\right) - \gamma \frac{B}{K_1 + B}P \quad \text{and} \quad 0 = \left(\beta\gamma \frac{B}{K_1 + B} - \delta\right)P.$$

The second equation of (2) at steady state can be solved for P; $P = \frac{r}{\gamma K}(K - B)(K_1 + B) =: F_1(B)$, having roots $B = K$ and $B = -K_1$. The solution $B = -K_1$ is

not biologically relevant and also is not within our invariant region Γ, as defined in the previous section. The other root, $B = K$, of $F_1(B)$ satisfies $\alpha(K) = 0$ only if $K \leq c$. The third equation at steady state can be solved as well; either $P = 0$ or $B = B_1 := \frac{\delta K_1}{\beta\gamma - \delta}$; with the latter being relevant only if $B_1 \leq c$, i.e. $\alpha(B_1) = 0$. To satisfy both equations at once, either $(B, P) = (0, 0)$, $(K, 0)$ or (B_1, P_1), where $P_1 = F_1(B_1)$. Thus, when $\alpha(B) = 0$, there are three possible steady states, all of which are disease free. The simplest equilibrium point occurs when $S = N$, $I = 0$, $B = 0$ and $P = 0$. The disease-free, bacteria-free and phage-free equilibrium $E_0 = (N, 0, 0, 0)$ is always an equilibrium of (2) for all parameter values. The disease-free, phage-free equilibrium denoted $E_K = (N, 0, K, 0)$ is an equilibrium if $K \leq c$. Similarly, if $B_1 \leq c$, then $\alpha(B_1) = 0$ and the disease-free equilibrium $E_1 = (N, 0, B_1, P_1)$ exists. However, for the positivity of P_1, we require that $B_1 < K$. Note that if $B_1 = K$, then $P_1 = 0$ and E_1 is simply E_K. The case of equilibria when $\alpha(B) \neq 0$ is more complicated, but it can be shown that there are up to two additional endemic equilibria denoted $E_{1,K}^* = (S_{1,K}^*, I_{1,K}^*, B_{1,K}^*, P_{1,K}^*)$ where all of the entries are strictly positive, making $E_{1,K}^*$ the only interior equilibria if they exist. If $\alpha(B^*) \neq 0$, first note that $B^* > c$ by definition. Dropping the asterisk on B, the first equation of (2) at equilibrium implies

$$I^* = G_1(B) := Na\frac{(B - c)}{(a + \mu)(B - c) + \mu H}.$$

So for each equilibrium value B^* such that $\alpha(B^*) \neq 0$, there exists a unique value $I^* = G_1(B^*)$. To find B^* and P^*, it is of no consequence that $I^* \neq 0$ because with $\xi = 0$, the second and third equations of (2) do not contain terms including I. Thus, the nontrivial values of (B, P) that satisfy the second and third equations at steady state are the same as before: $(B, P) = (K, 0)$ and (B_1, P_1), but now $K > c$ is required so that $\alpha(K) \neq 0$ and $B_1 > c$ so that $\alpha(B_1) \neq 0$. For the positivity of P_1, it is still necessary that $B_1 < K$. Summarizing, there are up to two endemic equilibria of (2), denoted $E_K^* = (S_K^*, I_K^*, K, 0)$ and $E_1^* = (S_1^*, I_1^*, B_1, P_1)$, where $I_K^* = G_1(K)$, $I_1^* = G_1(B_1)$ and $S_i^* = N - I_i^*$, $i = 1, k$, with the condition that $K > c$ and $c < B_1 < K$ for E_K^* and E_1^* to exist respectively. As seen above, if $B_1 = K$, then this would mean $P_1 = 0$ and $E_K^* = E_1^*$, leaving only one endemic equilibrium.

4.2 Linearization

Due to the threshold in the infection term, linearization yields two cases, one for $B^* \leq c$, denoted Jac_1, and one for $B^* > c$, denoted Jac_2:

$$\text{Jac}_1(I, B, P) = \begin{pmatrix} -\mu & 0 & 0 \\ 0 & r - 2\frac{r}{K}B - \frac{\gamma K_1}{(K_1+B)^2}P & -\gamma\frac{B}{K_1+B} \\ 0 & \beta\gamma\frac{aH}{(B-c+H)^2}P & \beta\gamma\frac{B}{K_1+B} - \delta \end{pmatrix},$$

and

$$\text{Jac}_2(I, B, P) = \begin{pmatrix} -\alpha(B) - \mu & (N-I)\frac{aH}{(B-c+H)^2} & 0 \\ 0 & r - 2\frac{r}{K}B - \frac{\gamma K_1}{(K_1+B)^2}P & -\gamma\frac{B}{K_1+B} \\ 0 & \beta\gamma\frac{aH}{(B-c+H)^2}P & \beta\gamma\frac{B}{K_1+B} - \delta \end{pmatrix}.$$

4.3 Stability of the Disease-Free, Bacteria-Free, Phage-Free Equilibrium E_0

Corresponding to E_0, we have the following eigenvalues: $\lambda = -\mu, -\delta < 0$ and $r > 0$. This means that the disease-free, bacteria-free and phage-free equilibrium E_0 is a saddle-node equilibrium with a one-dimensional unstable manifold.

4.4 Stability of the Disease-Free, Phage-Free Equilibrium E_K

Corresponding to E_K, we have the following eigenvalues: $\lambda = -\mu, -r, \beta\gamma\frac{K}{K_1+K} - \delta$. If $K < \frac{\delta K_1}{\beta\gamma-\delta} = B_1$, then all eigenvalues are negative and E_K is a stable equilibrium, but if $K > \frac{\delta K_1}{\beta\gamma-\delta} = B_1$, then E_K is a saddle-node equilibrium with a one-dimensional unstable manifold. Note that $B_1 < K$ is required for E_1 to exist, so the existence of E_1 and the stability of E_K are contrary notions.

4.5 Stability of the Disease-Free Equilibrium E_1

For the Equilibrium point E_1, we have the following Jacobian matrix:

$$\text{Jac}_1(0, B_1, P_1) = \begin{pmatrix} -\mu & 0 & 0 \\ 0 & r - 2\frac{r}{K}B_1 - \frac{\gamma K_1}{(K_1+B_1)^2}P_1 & -\gamma\frac{B_1}{B_1+K_1} \\ 0 & \beta\gamma\frac{K_1}{(K_1+B_1)^2}P_1 & 0 \end{pmatrix}.$$

The matrix is slightly more complicated, so we will use a lemma from McCluskey and van den Driessche (2004) with regard to three-dimensional matrices.

Lemma 2 (Lemma 3, McCluskey and Driessche 2004) *Let A be an 3×3 matrix with real entries. If $tr(A)$, $\det A$ and the determinant of the second additive compound matrix of A, $\det A^{[2]}$, are all negative, then all of the eigenvalues of A have negative real part.*

The converse of Lemma 2 is also true, which is apparent if you note that the eigenvalues of the second additive compound matrix $A^{[2]}$, for a 3×3 matrix A, are just $\sum \lambda_i + \lambda_j$ for $i < j$ with λ_i being the eigenvalues of A.

Defining $J(2,2) = r - 2\frac{r}{K}B_1 - \gamma\frac{K_1}{(K_1+B_1)^2}P_1$, the second additive compound of Jac_1 at E_1 is

$$\mathrm{Jac}_1^{[2]}(0, B_1, P_1) = \begin{pmatrix} -\mu + J(2,2) & -\gamma\frac{B_1}{B_1+K_1} & 0 \\ \beta\gamma\frac{K_1}{(K_1+B_1)^2}P_1 & -\mu & 0 \\ 0 & 0 & J(2,2) \end{pmatrix}.$$

The determinant of $\mathrm{Jac}_1(E_1)$ is

$$\det\mathrm{Jac}_1(E_1) = -\mu\gamma\frac{B_1}{B_1+K_1}\beta\gamma\frac{K_1}{(K_1+B_1)^2}P_1 < 0,$$

so it will always satisfy its role in the antecedent of Lemma 2. The trace is given by

$$tr(\mathrm{Jac}_1(0, B_1, P_1)) = -\mu + J(2,2).$$

If

$$J(2,2) < 0 \Rightarrow tr(\mathrm{Jac}_1) < 0,$$
$$J(2,2) > 0, -\mu + J(2,2) < 0 \Rightarrow tr(\mathrm{Jac}_1) < 0,$$
$$J(2,2) > 0, -\mu + J(2,2) > 0 \rightarrow tr(\mathrm{Jac}_1) > 0.$$

Finally, we need to consider the sign of $\det\mathrm{Jac}_1^{[2]}(E_1)$.

$$\det\mathrm{Jac}_1^{[2]}(E_1) = J(2,2)\left\{[-\mu + J(2,2)][-\mu] + \left(\beta\gamma\frac{K_1}{(K_1+B_1)^2}P_1\right)\left(\gamma\frac{B_1}{B_1+K_1}\right)\right\}.$$

We can see that if $J(2,2) < 0$, then $\det\mathrm{Jac}_1^{[2]} < 0$ and if $J(2,2) > 0$ but $J(2,2) - \mu < 0$, then $\det\mathrm{Jac}_1^{[2]} > 0$. If $J(2,2) > 0$ and $J(2,2) - \mu > 0$, then the antecedent of Lemma 2 will not be satisfied as $tr(\mathrm{Jac}_1(0, B_1, P_1)) > 0$. Thus, because $\det\mathrm{Jac}_1(0, B_1, P_1) < 0$ all the time, by Lemma 2, we have that

$$E_1 \text{ is stable} \iff J(2,2) < 0$$
$$\iff K < \frac{\beta\gamma + \delta}{\beta\gamma - \delta}K_1 = B_1 + \beta\gamma\frac{K_1}{\beta\gamma - \delta}$$

Define $B_3 = B_1 + \beta\gamma\frac{K_1}{\beta\gamma-\delta}$ and note that as we assume $\beta\gamma > \delta$, it follows that $B_3 > 2B_1$.

4.6 Stability of the Phage-Free Endemic Equilibrium E_K^*

Considering the equilibrium point E_K^*, we have that

$$
\mathrm{Jac}_2^{[2]}(E_K^*) = \begin{pmatrix} -\alpha(K) - \mu - r & -\gamma \frac{K}{K_1+K} & 0 \\ 0 & -\alpha(K) - \mu + \left(\beta\gamma \frac{K}{K+K_1} - \delta\right) & (N - I^*)\frac{aH}{(K-c+H)^2} \\ 0 & 0 & -r + \left(\beta\gamma \frac{K}{K+K_1} - \delta\right) \end{pmatrix}.
$$

$$
tr(\mathrm{Jac}_2(E_K^*)) = -\alpha(K) - \mu + \left(\beta\gamma \frac{K}{K+K_1} - \delta\right)
$$

with

$$
\det \mathrm{Jac}_2(E_K^*) = [-\alpha(K) - \mu][-r]\left[\beta\gamma \frac{K}{K_1+K} - \delta\right]
$$

and

$$
\det \mathrm{Jac}_2^{[2]}(E_K^*) = [-\alpha(K) - \mu - r]\left[-\alpha(K) - \mu + \beta\gamma \frac{K}{K+K_1} - \delta\right]
$$
$$
\left[-r + \beta\gamma \frac{K}{K_1+K} - \delta\right].
$$

Common to all three expressions is that if $K < B_1$, then they are each negative. And if $K > B_1$ then $\det \mathrm{Jac}_2$ at E_K^* is positive. Hence E_K^* is stable $\iff K < B_1$. Note that the stability condition of E_K^* is contrary to the existence condition for E_1^* and so there can only ever be at most one locally stable endemic equilibrium point at a time.

4.7 Stability of the Interior Endemic Equilibrium E_1^*

Finally, considering the local stability of interior endemic equilibrium E_1^*, we have that

$$
\mathrm{Jac}_2^{[2]}(I_1^*, B_1, P_1) = \begin{pmatrix} -\alpha(B_1) - \mu + J(2,2) & -\gamma \frac{B_1}{K_1+B_1} & 0 \\ \beta\gamma \frac{K_1}{(K_1+B_1)^2} P_1 & -\alpha(B_1) - \mu & (N - I^*)\frac{aH}{(B_1-c+H)^2} \\ 0 & 0 & J(2,2) \end{pmatrix}.
$$

$$
tr(\mathrm{Jac}_2(I_1^*, B_1, P_1)) = -\alpha(B_1) - \mu + J(2,2)
$$

and

$$
\det \mathrm{Jac}_2(I_1^*, B_1, P_1) = [-\alpha(B_1) - \mu]\gamma \frac{B_1}{B_1+K_1}\beta\gamma \frac{K_1}{(K_1+B_1)^2} P_1 < 0.
$$

So the determinant is always negative, and the trace can be negative if $J(2,2) < 0$. We now consider the sign of the determinant of $\mathrm{Jac}_2^{[2]}$ evaluate at (I_1^*, B_1, P_1).

$\det \operatorname{Jac}_2^{[2]}(I_1^*, B_1, P_1) = J(2,2)\left\{[-\alpha(B_1) - \mu + J(2,2)][-\alpha(B_1) - \mu] + \beta\gamma \frac{K_1}{(K_1+B_1)^2}\right.$

$\left. P_1\gamma \frac{B_1}{B_1+K_1}\right\}$ which appears complicated but the important part is that if $J(2,2) < 0$, then it will be negative. If $0 < J(2,2) < \alpha(B_1) + \mu$ implies that $\det \operatorname{Jac}_2^{[2]}(E_1^*) > 0$, and if $J(2,2) > \alpha(B_1) + \mu$ implies that both $\det \operatorname{Jac}_2^{[2]}(E_1^*) > 0$ and $tr(E_1) > 0$. As seen previously, $J(2,2) < 0$ is equivalent to $B_1 < B_3$, thus

$$E_1^* \text{ is stable} \iff B_1 < B_3 = B_1 + \frac{\beta\gamma}{\beta\gamma - \delta}.$$

4.8 Local Stability Summary, Bifurcation Diagrams and Numerical Simulations

Noting that there are at most 2 equilibria that exist at any one time other than E_0, and writing 'un' for locally unstable and 's' for locally asymptotically stable, we can summarize the preceding local stability results with a proposition.

Proposition 2 (Local stability of the non-shedding case) E_0 *always exists and is locally stable for all parameter values.*

If $c < K$	and $c \geq B_1$
	$B_3 \leq K$ implies E_1(un) and E_K^*(un) exist,
	$K < B_3$ implies E_1(s) and E_K^*(un) exist
	and $c < B_1$
	$K < B_1$ implies E_K^*(s) exists
	$B_1 < K < B_3$ implies E_K^*(un) and E_1^*(s) exist
	$B_3 \leq K$ implies E_K^*(un) and E_1^*(un) exist.
If $c \geq K$	and $c \geq B_1$
	$K < B_1$ implies E_K(s) exists
	$B_1 < K < B_3$ implies E_K(un) and E_1(s) exist
	$B_3 \leq K$ implies E_K(un) and E_1(un) exist
	and $c < B_1$
	as $B_1 < B_3$ then E_K(s) exists

The results of Proposition 2 are perhaps better understood as a bifurcation diagram. Figure 1 demonstrates the changes in stability as the carrying capacity K is varied. The first diagram is for the case when the minimum infectious dose c is greater than B_1, which means that only E_1 can exist, and not E_1^*. The lower figure has $c < B_1$, which reverses the situation.

If $K = B_3$, implying $J(2,2) = 0$, then computing $\det[\lambda I - \operatorname{Jac}_1(E_1)]$ we find that

$$\det(\lambda I - \operatorname{Jac}_1(E_1)) = (\lambda + \alpha(B_1) + \mu)\left\{\lambda^2 + \beta\gamma \frac{K_1}{(B_1+K_1)^2} P_1 \frac{\gamma B_1}{B_1 + K_1}\right\}$$

which has one real negative and two purely imaginary roots. We conclude that E_1 undergoes a Hopf bifurcation as K passes B_1, and E_1 changes from locally stable
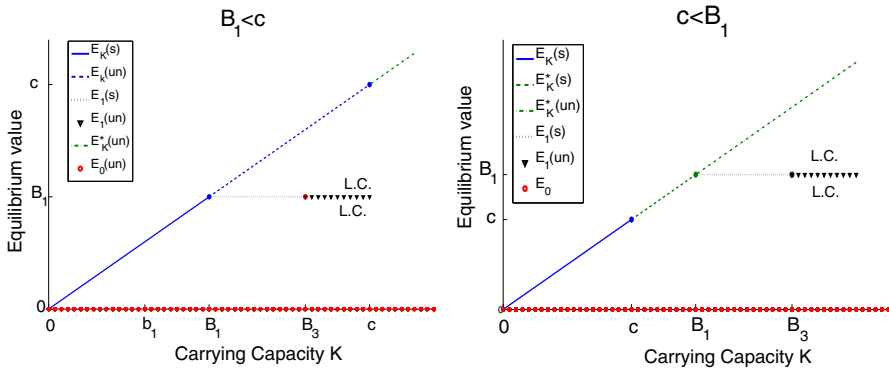
Fig. 1 Bifurcation diagrams when $\xi = 0$ and there is no shedding. Limit cycles exist when E_1 and E_1^* undergo Hopf bifurcations, and are denoted *L.C*
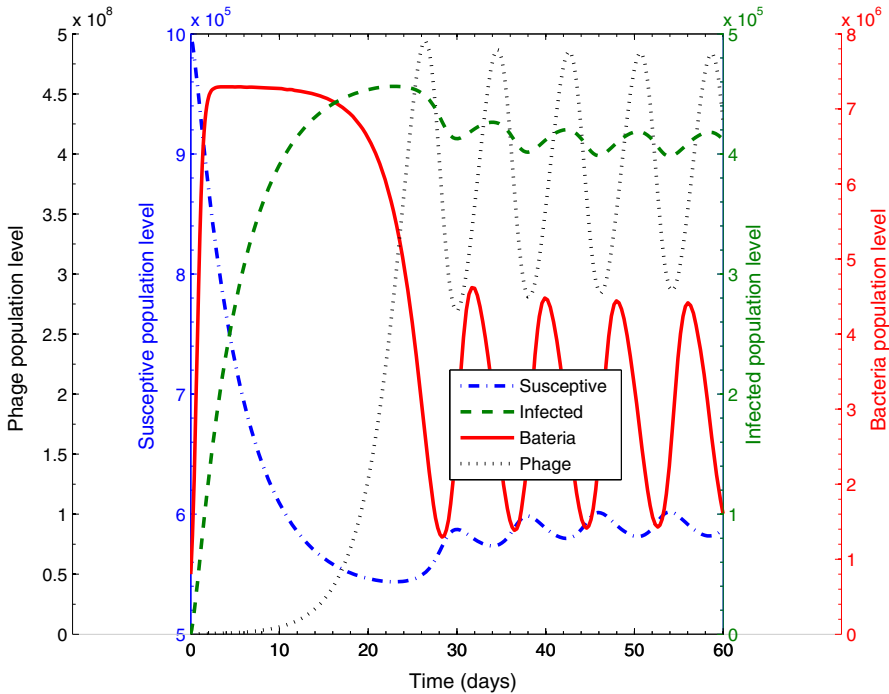
Fig. 2 Cycles in phage, bacteria and infected populations. The bacteria peak ends first, followed by the infected 4 days later and phage 8 days later. The parameters are $r = 3$, $K = 7.3e6$, $\gamma = 0.02$, $K_1 = 1.6e6$, $\beta = 80$, $\delta = 1$, $\xi = 0$, $a = 0.1$, $c = 7.1e6$, $\mu = 0.1$ and $H = 1e6$

to unstable. In Fig. 2, we demonstrate the existence of limit cycles occurring as a result of the unstable E_1. The stability conditions for the endemic equilibrium E_1^* are the same as for E_1, and it also undergoes a Hopf bifurcation when it exists and K increases past B_3. The only difference in the calculation of the eigenvalues of $\text{Jac}_2(E_1^*)$ is that the second entry in Jac_2 is nonzero, but as $\xi = 0$, the zeros in

the first column reduce the calculation of the eigenvalues of $\text{Jac}_2(E_1^*)$ to that shown above. When E_1 or E_1^* was unstable and the carrying capacity K was less than the MID (denoted c), cycles were observed numerically in the bacteria-phage system (BP) but not the susceptible-infected (SI) system. If K was sufficiently larger than c, implying that the MID was at a level such that bacteria at carrying capacity would cause infections, the cycles existed in both the SI and BP systems with the infected population peaking 4 days after and the phage population 8 days after in Fig. 2. While these cycles are far too short to match real world situations, as the infected class peaks occurred after the bacteria class, and because with shedding at zero the BP system influences the SI system unidirectionally, their existence does support the idea that cycles that naturally occur are bottom-up and not top-down in cause. When shedding is included, the cycles lengthen to relevant levels as we shall see in the next section.

5 Existence and Stability of Equilibria with Shedding

5.1 Existence of Equilibria

The complete absence of human contamination of the water supply is the ideal, but it is certainly not the reality anywhere and particularly not in places where the disease is endemic. Noting that the first equation of (1) is not necessary as $S + I = N$, we can rewrite it as follows:

$$
\begin{aligned}
\frac{dI}{dt} &= \alpha(B)(N - I) - \mu I, \\
\frac{dB}{dt} &= rB\left(1 - \frac{B}{K}\right) - \gamma\frac{B}{K_1 + B}P + \xi I, \\
\frac{dP}{dt} &= \beta\gamma\frac{B}{K_1 + B}P - \delta P + \phi\xi I.
\end{aligned}
\tag{3}
$$

If $\alpha(B) = 0$, then we will have the same endemic equilibria $E_0 = (N, 0, 0, 0)$, $E_K = (N, 0, K, 0)$ and $E_1 = (N, 0, B_1, P_1)$ as before, with the same conditions. If $\alpha(B) \neq 0$ at steady state, then from the first equation of (3), we have that $I^* = G_1(B^*) = \frac{Na(B^*-c)}{(a+\mu)(B^*-c)+\mu H}$, and from the third equation, we have that $P^* = \frac{-\phi\xi I^*}{\beta\gamma\frac{B^*}{K_1+B^*}-\delta} = \frac{-\phi\xi G_1(B^*)(K_1+B^*)}{\beta\gamma B^*-\delta(K_1+B^*)}$. This expression for P^* provides a condition for B^* as the denominator must be strictly negative in order to have a well-defined and positive value for P^*. That is, $B^* < \frac{K_1\delta}{\beta\gamma-\delta} = B_1$. Solving the second equation of (3) at equilibrium for B^*, assuming that $\alpha(B) \neq 0$, will then possibly lead to endemic equilibria E^*. Dropping the asterisks on B^* for convenience, the second equation at steady state becomes

$$
0 = rB\left(1 - \frac{B}{K}\right) + \xi I^* - \gamma\frac{B}{K_1 + B}P^* = F(B) + G(B),
\tag{4}
$$

Table 2 Possible ordering of $\{B_2, B_1, K, b_1, c\}$

Case	Subcase	Ordering
(Ia)		
$0 < B_2 < B_1 < K$	(i) $B_2 < b_1 < B_1$	$B_2 < b_1 < c < B_1$
		$B_2 < c < b_1 < B_1$
	(ii) $0 < b_1 < B_2$	$b_1 < B_2 < c < B_1$
(Ib)		
$0 < B_2 < K < B_1$	(i) $b_1 > K$	$K < c < b_1 < B_1$
		$c < K < b_1 < B_1$
	(ii) $B_2 < b_1 < K$	$B_2 < b_1 < c < K$
		$B_2 < c < b_1 < K$
	(iii) $b_1 < B_2$	$b_1 < B_2 < c < K < B_1$
(Ic)		
$K < B_2 < B_1$	(i) $B_2 < b_1 < B_1$	$B_2 < c < b_1 < B_1$
(IIa)		
$B_2 < 0 < B_1 < K$	(i) $b_1 < B_1$	$b_1 < c < B_1 < K$
		$c < b_1 < B_1 < K$
(IIb)		
$B_2 < 0 < K < B_1$	(i) $K < b_1$	$K < c < b_1 < B_1$
		$c < K < b_1 < B_1$
	(ii) $b_1 < K$	$b_1 < c < K < B_1$
		$c < b_1 < K < B_1$

The first column determines the order of $\{B_2, B_1, K\}$, the second places b_1 in that ordering and the third column places c within the ordering

where

$$F(B) := rB\left(1 - \frac{B}{K}\right)[(a + \mu)(B - c) + \mu H][(\beta\gamma - \delta)B - \delta K_1)]$$

$$G(B) := Na\xi[\gamma(\phi + \beta)B - \delta K_1 - \delta B](B - c).$$

Note that $F(B)$ is a quartic with roots 0, K, $B_2 := c - \frac{\mu H}{a+\mu}$ and B_1 which was defined previously as $B_1 = \frac{\delta K_1}{\beta\gamma - \delta}$, which opens downwards. The three roots of 0, B_1 and K are nonnegative, but B_2 could be negative or zero with realistic parameters. To solve $0 = F(B) + G(B)$, it suffices to find the intersections of $F(B)$ and $-G(B)$. As such note that $-G(B)$ is a downward opening parabola, with roots c and $b_1 := \frac{\delta K_1}{\gamma(\phi+\beta)-\delta}$.

The roots of the two functions have some obvious relationships which limit the number of possibilities we need to consider when looking for points where the two functions intersect. Consider b_1 and B_1, which are clearly related. We assume $\beta\gamma - \delta > 0$ and as $\phi > 0$, being part of the shedding term for the phage population $\phi\xi$; it is clear that $0 < b_1 < B_1$. Also, $B_2 < c$ as all parameter values are positive. Previously, we found that $c < B^* < B_1$ to ensure $P^* > 0$ and $\alpha(B^*) > 0$, so this implies that $c < B_1$ is a condition for any B^* to exist.

Between the third and fourth roots of F, we see that $F(B) > 0$, whatever those roots may be. If the largest root is B_1, then we find a problem if c is the next largest of $\{b_1, c, K, B_1, B_2\}$. As $-G(c) = 0$ with $-G(B) < 0$ for $B \geq c$, and $F(c) > 0$, then clearly no intersections can occur until $B > B_1$ when $F(B)$ is no longer nonnegative. Any such intersection would be inadmissible as $B^* > B_1$ for that B^*. Also, any intersections between F and $-G$ with $B < c$ are also inadmissible as we require $B^* > c$. Hence, if $c < B_1$ and $\{c, B_1\}$ are the largest of $\{b_1, c, K, B_1, B_2\}$, then there will be no endemic equilibria.

The possible orderings of $\{B_2, B_1, K, b_1, c\}$ are outlined in Table 2. There are only 9 combinations of $\{B_2, B_1, K, b_1\}$ and 15 orderings of all of the roots of F and G when all of the restrictions are considered. There can be up to 4 equilibria at one time depending on the relationships among the parameters. We can summarize these results with a proposition.

Proposition 3 (Existence of Equilibria) *The equilibrium $E_0 = (N, 0, 0, 0)$ always exists.*

If $c \geq K$	and $B_1 \leq c$,
	if also $B_1 > K$, then only E_K exists.
	if $B_1 \leq K$ then E_K and E_1 exist.
	and $B_1 > c$,
	if $c < b_1$ then there are up to $B^*_{1,2} \in (c, b_1)$ and E_K.
	if $c > b_1$ then there are no internal equilibria but E_K exists.
If $c < K$	and $B_1 > c$
	then B^* exists between the second and third in the ordering of $\{c, K, b_1, B_1\}$.
	and $B_1 \leq c$
	there are no internal equilibria and E_1 is an equilibrium.

5.2 Linearization

Due to the threshold in $\alpha(B)$, we will have two linearizations of (3) with the first having $\alpha(B) = 0$, denoted J_1:

$$J_1(I, B, P) = \begin{pmatrix} -\mu & 0 & 0 \\ \xi & r - 2\frac{r}{K}B - \frac{\gamma K_1}{(K_1+B)^2}P & -\gamma\frac{B}{K_1+B} \\ \phi\xi & \beta\gamma\frac{aH}{(B-c+H)^2}P & \beta\gamma\frac{B}{K_1+B} - \delta \end{pmatrix},$$

and the second linearization applies when $\alpha(B) \neq 0$, denoted J_2

$$J_2(I, B, P) = \begin{pmatrix} -\alpha(B) - \mu & (N - I)\frac{aH}{(B-c+H)^2} & 0 \\ \xi & r - 2\frac{r}{K}B - \frac{\gamma K_1}{(K_1+B)^2}P & -\gamma\frac{B}{K_1+B} \\ \phi\xi & \beta\gamma\frac{aH}{(B-c+H)^2}P & \beta\gamma\frac{B}{K_1+B} - \delta \end{pmatrix}.$$

5.3 Stability of Disease-Free, Bacteria-Free, Phage-Free Equilibrium E_0

Corresponding to E_0, we have the following eigenvalues $-\mu, -\delta < 0$ and $r > 0$. This means that the equilibrium E_0 is a saddle-node equilibrium with a one-dimensional unstable manifold.

5.4 Stability of the Boundary Equilibrium E_K

Considering the equilibrium point E_K, we have that

$$J_1^{[2]}(0, K, 0) = \begin{pmatrix} -\mu - r & \left(-\gamma \frac{K}{K_1+K}\right) & 0 \\ 0 & -\mu + \beta\gamma \frac{K}{K_1+K} - \delta & 0 \\ -\phi\xi & \xi & -r + \left(\beta\gamma \frac{K}{K_1+K} - \delta\right) \end{pmatrix}$$

$tr(J_1(0, K, 0)) = -\mu - r + \left(\beta\gamma \frac{K}{K_1+K} - \delta\right)$, $\det J_1(0, K, 0) = \mu r \left(\beta\gamma \frac{K}{K_1+K} - \delta\right)$ and $\det J_1^{[2]} = (-\mu-r)\left(-\mu + \beta\gamma \frac{K}{K_1+K} - \delta\right)\left(-r + \beta\gamma \frac{K}{K_1+K} - \delta\right)$. If $\beta\gamma \frac{K}{K_1+K} - \delta < 0$ this implies that $tr(J_1)$, $\det J_1$ and $\det J_1^{[2]}$ are all negative, but if $\beta\gamma \frac{K}{K_1+K} - \delta > 0$, then $\det J_1 > 0$. By Lemma 2, this means that E_K is stable if and only if $K < \frac{\delta K_1}{\beta\gamma-\delta} = B_1$. Note that $B_1 < K$ is required for E_1 to exist, so the existence of E_1 and the stability of E_K are contrary notions.

5.5 Stability of the Disease-Free Equilibrium E_1

Defining $J(2, 2) = r - 2\frac{r}{K}B_1 - \gamma \frac{K_1}{(K_1+B_1)^2} P_1$ again as in the previous non-shedding case, the second additive compound matrix of J_1 is

$$J_1^{[2]}(0, B_1, P_1) = \begin{pmatrix} -\mu + J(2, 2) & -\gamma \frac{B_1}{B_1+K_1} & 0 \\ \beta\gamma \frac{K_1}{(K_1+B_1)^2} P_1 & -\mu & 0 \\ -\phi\xi & \xi & J(2, 2) \end{pmatrix}.$$

The determinant of J_1, $\det J_1(0, B_1, P_1)$, < 0, so it will always satisfy the antecedent of Lemma 2. The trace is given by $tr(J_1(0, B_1, P_1)) = -\mu + J(2, 2)$. As before $J(2, 2) < 0$ if and only if, $K < B_3 = B_1 + \frac{\beta\gamma K_1}{\beta\gamma-\delta}$. If

$$J(2, 2) < 0 \Rightarrow tr(J_1) < 0$$
$$J(2, 2) > 0, -\mu + J(2, 2) < 0 \Rightarrow tr(J_1) < 0$$
$$J(2, 2) > 0, -\mu + J(2, 2) > 0 \to tr(J_1) > 0.$$

Finally, consider the sign of det $J_1^{[2]}$

$$
\det J_1^{[2]}(0, B_1, P_1) = J(2, 2) \left\{ [-\mu + J(2, 2)][-\mu] \right.
$$
$$
\left. + \left(\beta\gamma \frac{K_1}{(K_1 + B_1)^2} P_1 \right) \left(\gamma \frac{B_1}{B_1 + K_1} \right) \right\},
$$

where it is clear that if $J(2, 2) < 0$ then $\det J_1^{[2]} < 0$ and if $J(2, 2) > 0$ but $J(2, 2) - \mu < 0$ then $\det J_1^{[2]} > 0$. If $J(2, 2) > 0$ and $J(2, 2) - \mu > 0$, then the antecedent of Lemma 2 will not be satisfied as $tr(J_1(0, B_1, P_1)) > 0$. Thus, since $\det J_1(0, B_1, P_1) < 0$ all the time, by Lemma 2, we have that E_1 is stable $\iff$ $J(2, 2) < 0$ i.e E_1 is stable if and only if $K < \frac{\beta\gamma+\delta}{\beta\gamma-\delta} K_1 = B_1 + \beta\gamma \frac{K_1}{\beta\gamma-\delta} = B_3$

5.6 Stability of Endemic Equilibria E^* and $E_{1,2}^*$

The stability of the endemic steady states was found numerically. If $c > b_1$ and $c < B_1$, then there is a unique endemic equilibrium, E^*. Using parameter values, $r = 1, \gamma = 0.02, K_1 = 3.6e5, \beta = 80, \delta = 1, \xi = 50, \phi = 1, a = 0.1, H = 1e6, c = 5.9e5$ and $\mu = 0.1$ will achieve such a relationship. If $K = 7e5 > c$ or larger, E_K does not exist, and E_0 and E^* are the only equilibria. Limit cycles are observed, and if B^* and its eigenvalues are computed numerically, then we see that E^* is a saddle-node equilibrium with a two-dimensional unstable manifold.

If $K = 4e5 < c = 5e5$, with all other parameters the same, then $K < c < b_1$ and two endemic equilibria exist, along with E_0 and E_K. In this case, they are both saddle-node equilibria, where E_1^* (with the smaller B^* value) has a one-dimensional unstable manifold, and the other has a two-dimensional unstable manifold. If $K = 5.9e5 > c$ or greater, then there is a unique endemic equilibria and E_K no longer exists. As before, it is a saddle-node with two-dimensional unstable manifold.

Finally, if K_1 is decreased to $K_1 = 1.6e5$, with all other parameters as before, and if $c > b_1$ and the endemic equilibrium is unique, then it is again a saddle-node with two-dimensional unstable manifold. If instead $c < b_1$, then when the two internal equilibria exist, E_1^* (with the smaller B^*) is a saddle-node with one-dimensional unstable manifold as before. The larger, however, is stable as its eigenvalues all have negative real part. Finally, if $K > c$, for example $K = 2.2e6$ or higher, then there is a unique endemic equilibrium E^* which is locally stable as all eigenvalues have negative real part.

5.7 Local Stability Summary, Bifurcation Diagrams and Numerical Simulations

We can summarize the local stability results of the previous sections with a proposition, writing 'un' for locally unstable, and 's' for local asymptotic stability. The goal of the bifurcation diagrams below was to exhibit all possible cases of the model, and thus their associated parameter ranges are wider than the variation of parameter values in simulations.

Proposition 4 (Local Stability) E_0 *is always locally unstable.*

If $c \geq K$	and $B_1 \leq c$,
	if $K > B_3$, then E_1(un) and E_K(un).
	if $B_1 < K < B_3$ then E_1(s) and E_K(un).
	if $K < B_1$ then E_K(s).
	and $B_1 > c$,
	if $c < b_1$ then there are up to $E_{1,2}^*$ and E_K(s),
	with $B_i^* \in (c, b_1)$.
	if $c > b_1$ then there are no internal equilibria but E_K(s).
If $c < K$	and $B_1 > c$,
	then E^* exists,
	with B^* between the second and third in the ordering of $\{c, K, b_1, B_1\}$.
	and $B_1 \leq c$,
	if $K > B_3$, then E_1(un).
	if $K < B_3$, then E_1(s).

In addition to the infection-free, bacteria-free and phage-free equilibrium E_0, which always exists and is always locally unstable, there are at most three other equilibria for any given set of parameters. Note that E_1 and E_K are never both stable at the same time, as the condition for the local stability of E_K implies that E_1 does not exist. Of the two, E_1 is more realistic as it has the phage population existing at nonzero levels, which is certainly the case during inter-epidemic times. The existence of a stable endemic equilibrium, either when E^* is unique, or when it exists with another, which is unstable, does not match the usual pattern of explosive outbreaks of cholera, but if the B^* level is low enough, perhaps it could be biologically relevant for certain areas. Our main interest is on the existence of limit cycles, as will be discussed below. The results of Proposition 4 are perhaps better understood with bifurcation diagrams. Figure 3 shows the case when $B_1 < c$, and only nonendemic equilibria are possible. In the figure, $B_3 < c$, which means that both E_1 and E_K can be unstable at the same time. If this was reversed and $B_3 > c$, then the difference would be that E_1 would be unstable only when E_K does not exist, and the two could not be unstable for the same set of parameters.

Equilibrium E_1 is only present in the first diagram, and when the carrying capacity $K = B_3$, we can calculate $\det[\lambda I - J_1(E_1)]$, noting that $J(2, 2) = 0$ to see that

$$\det[\lambda I - J_1(E_1)] = (\lambda + \mu) \left\{ \lambda^2 + \beta \gamma \frac{K_1}{(K_1 + B_1)^2} P_1 \gamma \frac{B_1}{B_1 + K_1} \right\},$$

and observe that $J_1(E_1)$ would have one negative eigenvalue and two purely imaginary eigenvalues. Thus, E_1 undergoes a Hopf bifurcation as K increases past B_3 and E_1 switches from locally stable to unstable. With parameters in the region where E_1 is
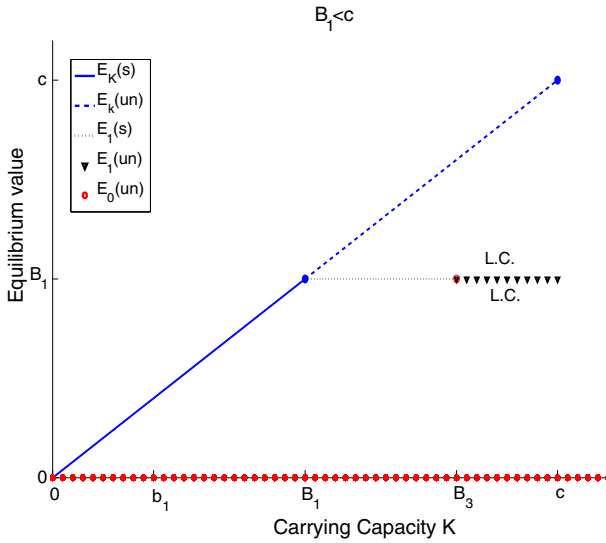
Fig. 3 Bifurcation diagrams with all parameters positive and $B_1 < c$, which implies only nonendemic equilibria exist. Equilibrium E_1 undergoes a Hopf bifurcation when carrying capacity K increases past B_3, leading to limit cycles denoted $L.C$

unstable, we found limit cycles to exist. If $K < c$, then these cycles existed only in the BP community and did not cause any infections. Figure 4 demonstrates such limit cycles, with period of only 14 days, and phage peaking 5 days after the bacteria class does. If $K > c$ by a large enough amount, meaning that the minimum infectious dose is less than the normal carrying capacity of bacteria, the cycles entered the human population as well and increase greatly in period. Unlike the case with $\xi = 0$, the period of these cycles could even be approximately 180 days, which could correspond to the biannual outbreaks observed in some endemic areas. Figure 5 is an example of such cycles with period of *150 days*. The bacteria are the first to peak, followed by the human-infected population 3 days later, and the phage 1 day after the infected class. As these cycles can exist at low levels and only enter the human population when the bacteria levels increase passed the MID, and because the bacteria peak before the infected human population, we conclude that the BP system is 'driving' these limit cycles.

Figure 6 contains bifurcation diagrams for the cases of endemic equilibria. The first diagram of Fig. 6 is for when E^* is unique, and numerically, it was found to always be unstable and causing limit cycles. The second diagram is very similar, except that up to two $E^*_{1,2}$ can exist. These are either both unstable, or the equilibrium with the smaller B^*_i value was unstable and the larger was stable. The unique E^* in the second diagram could be either stable or unstable for realistic parameter values, and when it was unstable, limit cycles were found to exist. These cycles ranged in period, but could be found with periods of approximately 360 days, as in Fig. 7, which correspond to the annual outbreaks observed in some endemic areas. The period of outbreaks and maximum number of people infected in an outbreak differ from one endemic region to another depending largely on sanitational infrastructures. Figure 8a shows that whenever an outbreak occurs in an endemic/epidemic region with poor sanitational infrastructures,
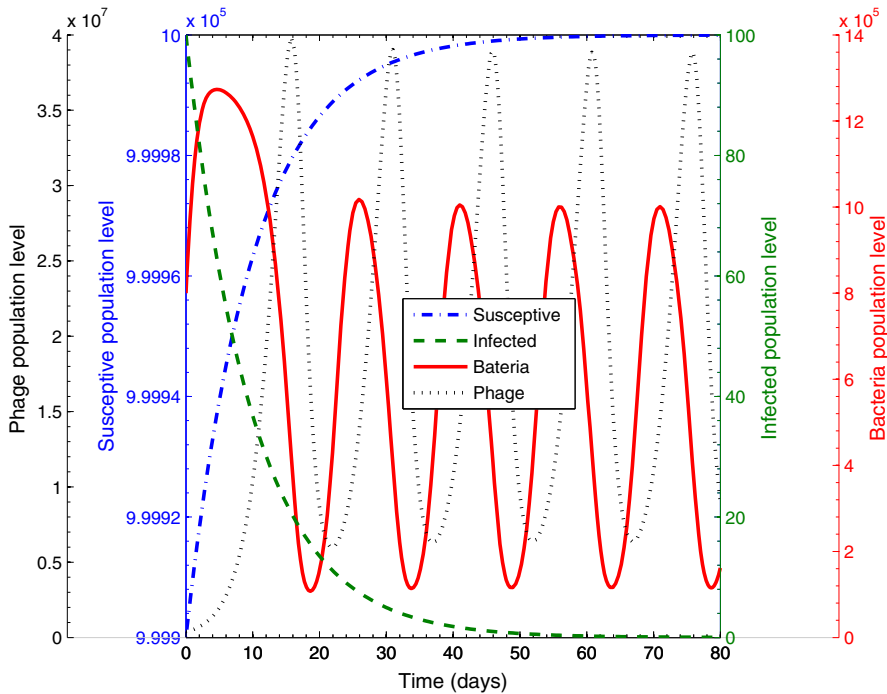
Fig. 4 Dynamics of I, S, B and P when E_1 is unstable and $K < c$. When the bacteria levels pass the minimum infectious dose (MID), the cycles spread to the human population as well. The period is approximately 15 days and the phage peak 4 days the bacteria. The parameters are $r = 1$, $K = 1.3e6$, $\gamma = 0.02$, $K_1 = 2.5e5$, $\beta = 80$, $\delta = 1$, $\xi = 50$, $\phi = 1$, $a = 0.1$, $H = 1e6$, $c = 1.5e6$ and $\mu = 0.1$

many people are infected compared to when it occurs in an endemic region with better sanitational infrastructures. The number of infected persons increases monotonically as ξ increases from 0 to 300. Thus, improving the sanitational infrastructure of an endemic region could lead to a reduction in the number of infected persons whenever an outbreak occurs. This alone is unable to eradicate cholera. Figure 8b shows the effect of poor sanitational infrastructure on the period of the outbreaks. By increasing ξ from 0 to 300, the period of the outbreaks decreases monotonically as ξ moves from 0 to 15 and attends a minimum value of approximately 346 days, and thereafter increases monotonically as ξ goes above 15. The fact that the period of the outbreaks decreases as the shedding rate increases from 0 to 15 is counterintuitive.

6 Chaos

In this section, we will attempt an explanation to the different natures of the outbreak experience around the world. We will attempt to explain why you might have countries with the same sanitational infrastructure but the outbreak in one might be sporadic, whereas those in the other are periodic. For instance, Malaysia and Zambia have approximately the same sanitational infrastructure but the outbreaks in Malaysia are sporadic, whereas those in Zambia are periodic.
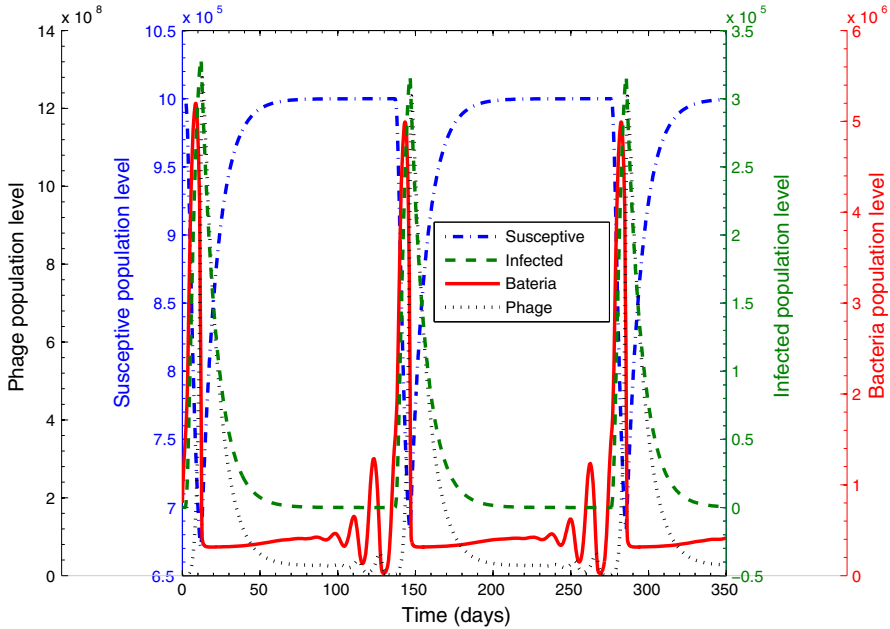
Fig. 5 Dynamics of I, S, B and P when E_1 is unstable and $K > c$. When the bacteria levels pass the minimum infectious dose (MID), the cycles spread to the human population as well. The infected class peaks 3 days after the bacteria, and the phage 4 days after. The parameters are $r = 1$, $K = 1.8e6$, $\gamma = 0.02$, $K_1 = 2.5e5$, $\beta = 80$, $\delta = 1$, $\xi = 50$, $\phi = 1$, $a = 0.1$, $H = 1e6$, $c = 1.5e6$ and $\mu = 0.1$. The period is approximately 150 days, which corresponds to biannual outbreaks in endemic areas
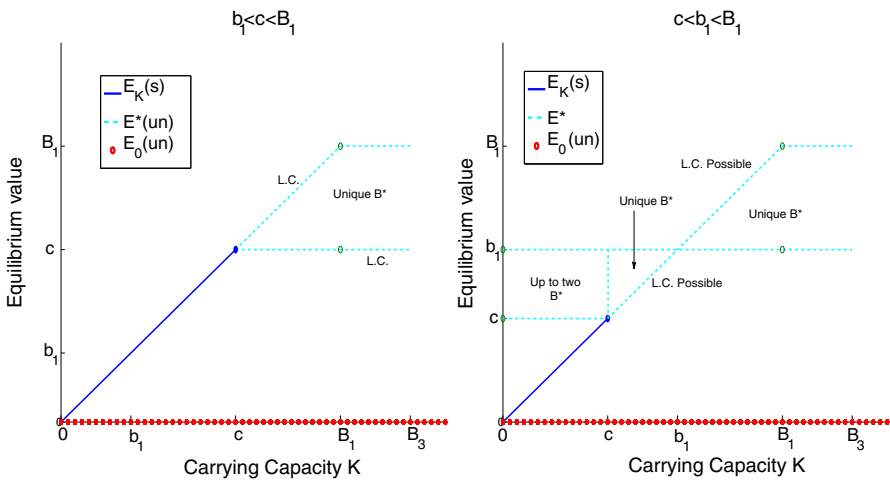
Fig. 6 Bifurcation diagrams with all parameters positive. Limit cycles exist after when E^* is unique and unstable and are denoted $L.C.$ When $c > b_1$, E^* was always unstable, and there were cycles. When $c < b_1$, these cycles existed when E^* was unstable, but were absent when it was stable. If there were two equilibria $E_{1,2}^*$, then they were either both unstable, or the one with the smaller B_i^* was unstable and the larger was stable. Limit cycles were not observed with parameters in this range
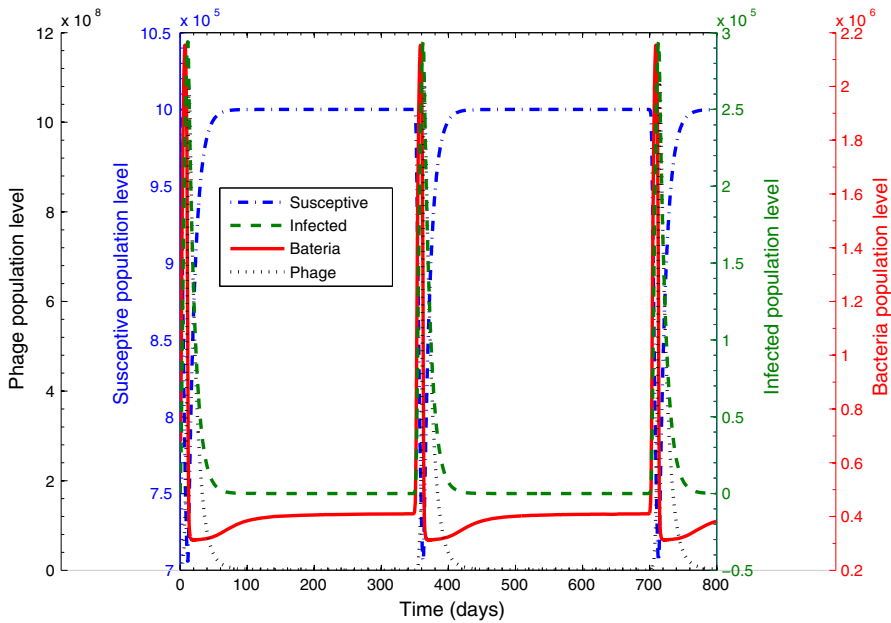
Fig. 7 Dynamics of I, S, B and P when E^* is unique and unstable with $K > c$. When the bacteria levels pass the minimum infectious dose (MID), the cycles spread to the human population as well. The infected class peaks 3 days after the bacteria, and the phage 6 days after. The parameters are $r = 1$, $K = 4.12e5$, $\gamma = 0.02$, $K_1 = 2.5e5$, $\beta = 80$, $\delta = 1$, $\xi = 50$, $\phi = 1$, $a = 0.1$, $H = 1e6$, $c = 4.1e5$ and $\mu = 0.1$. The period is approximately 351 days, which corresponds to annual outbreaks in endemic areas

In many countries that experience endemic cholera, there are annual cholera outbreaks which appear to be periodic. However, in countries with similar sanitation infrastructure, the outbreaks are much more frequent and lack an overwhelmingly periodic structure. The general trend is that countries closer to the equator have higher levels of outbreaks with greater frequency, while countries that are farther from the equator typically have seasonal outbreaks (Emch et al. 2008). An explanation for this trend may lie in the existence of chaotic behaviour in (1) for certain values of the shedding parameters ξ and ϕ. This window of chaos depends on other parameters in (1) as well, and not just ξ and ϕ. The maximal growth rate of bacteria r is proportional to the values ξ_c and ϕ_c where chaos first occurs. If this value of r is itself proportionate to average temperatures, and thus inversely proportional to the distance from the equator, then warmer countries with a higher r value could have chaotic behaviour of bacterial levels, and thus outbreaks with the same values of ξ and ϕ. A positive relationship between bacteria proliferation and average temperature is known to exist, so this explanation is plausible (Singleton et al. 1982). Figure 9 demonstrates different trends in cholera outbreaks for countries at different latitudes. Malaysia for example is the closest to the equator of the four countries shown, at a latitude of 4°, and has a somewhat uniform distribution of monthly outbreaks when summed over 32 years. The other three countries of Romania, Iran and Zambia, which are at a distance of at least ±13° from the equator, have much stronger trends in what month cholera outbreaks typically
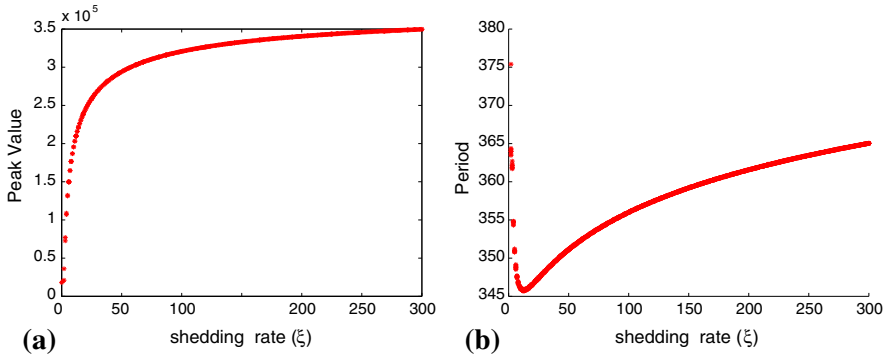
Fig. 8 The parameters are $r = 1$, $K = 4.12e5$, $\gamma = 0.02$, $K_1 = 2.5e5$, $\beta = 80$, $\delta = 1$, $\phi = 1$, $a = 0.1$, $H = 1e6$, $c = 4.1e5$ and $\mu = 0.1$. For these parameter values, each ξ value leads to an oscillating trajectory with a unique period. **a** The effect of an increase in ξ on the peak value of I cycles when E^* is unique and unstable with $K > c$. **b** The effect of an increase in ξ on the period of outbreaks when E^* is unique and unstable with $K > c$
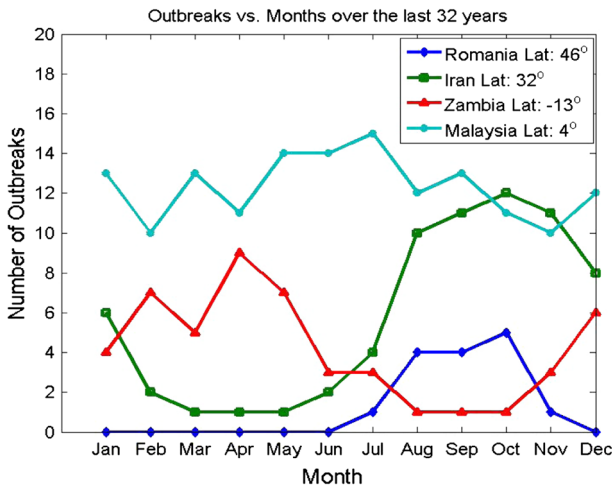
Fig. 9 (Color Figure Online) Sums of monthly cholera outbreaks over the last 32 years in countries at different latitudes, adapted from Emch et al. (2008)

occur. For Romania and Iran, which are both in the Northern Hemisphere, outbreaks typically occur between August and November. In Zambia, which is in the Southern Hemisphere, outbreaks occur most often between February and May. A larger value of the maximal bacterial growth rate r for countries closer to the equator, which also corresponds to a lower value of ξ_c and ϕ_c, could explain why the outbreaks in warmer countries occur less seasonally than in countries further away from the equator.

In the panels (a) and (d) of Fig. 10, the shedding rate ξ is increased by 0.01 after each time step, and for each value, the peak values of the trajectory produced are numerically determined and used to estimate the length of each cycle in it. For the
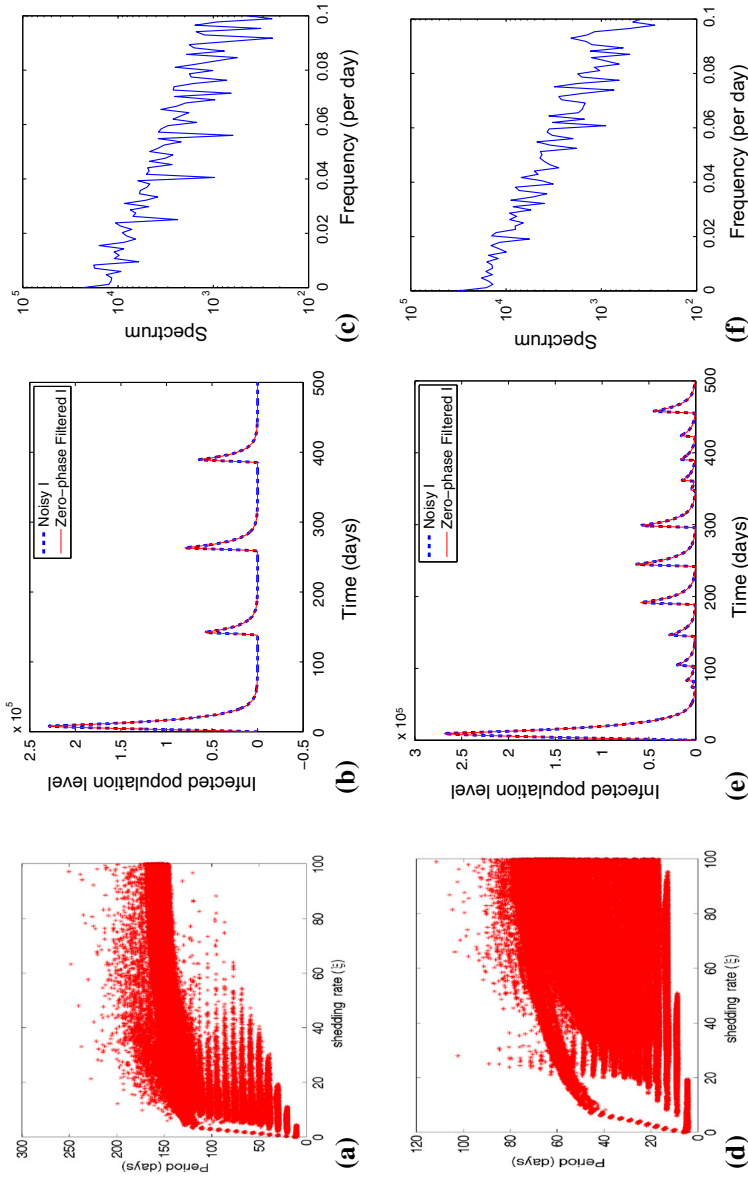
Fig. 10 (Color Figure Online) Chaotic behaviour with two different r (maximum bacterial growth) values. The remaining parameters are $K = 1e6$, $\gamma = 0.021$, $K1 = 1/4K$, $\beta = 100$, $\delta = 1$, $\phi = 0$, $a = 0.1$, $c = 5e5$, $\mu = 0.1$, $H = 1e6$. **a** shedding rate vs. period with $r = 1$, **b** trajectory for $r = 1$ and $\xi = 11$, **c** single-sided amplitude spectrum of filtered I with r=1, $\xi = 11$, **d** shedding rate vs. period with $r = 5$, **e** trajectory for r=5 and $\xi = 53$, **f** single-sided amplitude spectrum of filtered I with $r = 5$, and $\xi = 53$
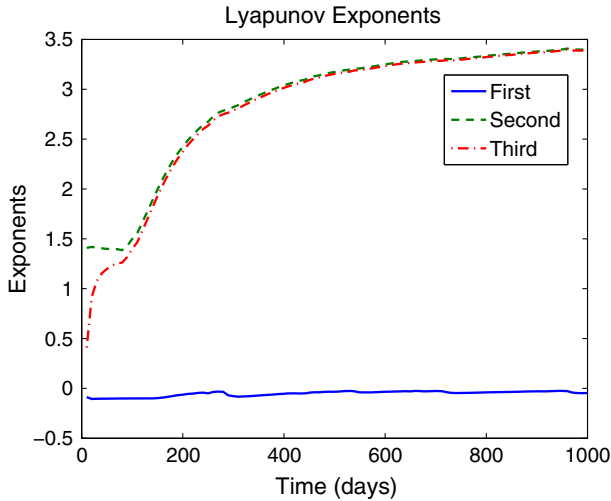
Fig. 11 (Color Figure Online) Lyapunov exponents for (1). The parameters used are the same as those in Fig. 10a with $\xi = 11$. The largest is positive which is enough to determine that the trajectory is chaotic

maximal growth rate r comparatively low, we have trajectories oscillating with varying peak values and periods occurring for lower values of ξ. In Fig. 10a, r is comparatively low and for most values of ξ approximately less than 30, the corresponding trajectory has varying periods (See Fig. 10b for the behaviour of the trajectories for a typical ξ in this interval). On the contrary, for r comparatively high, oscillating trajectories with varying peak values and periods occur for higher values of ξ as can be seen in Fig. 10d where $r = 5$ and for ξ approximately greater than 20, the trajectory for each ξ has varying peak values and length of cycles (see Fig. 10f for the behaviour of the trajectories for a ξ taken from this interval). Thus, the same values of ξ and ϕ could cause different trajectories for different values of r. In Fig. 10, it is the unstable E_1 that causes the cycles, but an unstable E^* could also be used. Figure 10c and e presents the Fast Fourier Transform (FFT) of the filtered infected population trajectories in Fig. 10b and f, respectively. These FFT show continuous spectrum of frequencies. This behaviour is typical of chaotic motions. However, it is not enough to determine if the behaviour is chaotic: we should consider the Lyapunov Exponents. In Fig. 11, we see that due to the positivity of the largest Lyapunov exponent, the behaviour is in fact chaotic. Furthermore, the largest two exponents are both positive and almost the same value. They correspond to the bacteria and phage categories from the model, which suggests that it is the bacteria-phage system which drives the cyclic behaviour of the entire system, and that they are the most sensitive to perturbations.

7 Discussion

We have presented a model, which is an extension of the one in Jensen et al. (2006). This model explicitly includes the dynamics of bacteriophage and bacteria, and also contains a new indirect infection term which accounts for a minimum infectious dose

of the pathogen *V. cholerae*. Unlike Jensen et al. (2006), we focused on the existence of stable limit cycles, in order to account for the periodicity observed in outbreaks of cholera in endemic areas. As these cycles exist in the absence of human contribution to the bacteria and phage levels, and because the bacteria cycles peak before the human cycles when they exist in both systems, we conclude that it is the bacteria and phage which are driving the cycles, and not the reverse situation. If the minimum infectious dose is less than the carrying capacity of the bacteria, then we observe that the bacteria cycles usually fail to surpass the minimum infectious dose, so there are no new infections and the system is disease free. However, if the natural carrying capacity is sufficiently larger than the minimum infectious dose, then these cycles are able to enter the human population, which highlights the importance of understanding the relationship between the two. Additionally, as a control measure, if the phage levels could be enhanced in some way to keep the bacteria below this minimum infectious dose, then the cycles would remain in the bacteria and phage system alone. This idea links back to the 1930s when the use of injections of bacteriophage was explored as a treatment of cholera by limiting *V. cholerae* levels within the human host (Asheshov and Lahiri 1931; Pasricha et al. 1936).

Additionally, a chaotic region in the parameter space was identified. The existence of chaotic behaviour could explain the lack of clear periodicity in some endemic areas, with seasonal or other factors increasing the height of these chaotic peaks annually or biannually and creating a pseudo-periodic pattern. The exact role of these external factors would be difficult to determine, given the sensitivity of such a system. As the existence of this chaotic parameter region can be positively correlated with the proliferation rate of *V. cholerae* and overall climate, it could also explain the unpredictable nature of outbreaks in countries nearer to the equator.

Some of the work in this manuscript is part of the Master's thesis of the second author, Davis (2012).

Future work on the model could be to explicitly include the role of infection-derived immunity through the use of a recovered class, even though immunity is somewhat accounted for the value of the minimum infectious dose. Exact conditions for the existence of limit cycles would be valuable as well as a definitive relationship between the amplitude and period of the cycles to other parameters in the system. This would be useful in establishing useful connections between simulations and the data. Furthermore, including a second disease causing serogroup of *V. cholerae* would increase the realism of the model for use in regions where outbreaks caused by serogroups O1 and O139 occur simultaneously.

References

Asheshov I, Lahiri MN (1931) The treatment of cholera with bacteriophage. Ind Med Gaz 66:179–184
Baker RM, Singleton FL, Hood MA (1983) Effects of nutrient deprivation on *Vibrio cholerae*. Appl Environ Microbiol 46:930–940

Capasso V, Paveri-Fontana SL (1979) A mathematical model for the 1973 cholera epidemic in the European Mediterranean region. Rev Epidemiol Sante Publique 27:121–132

Cash RA, Music SI, Libonati JP, Snyder MJ, Wenzel RP, Hornick RB (1974) Response of man to infection with *Vibrio cholerae*. I. Clinical, serologic, and bacteriologic responses to a known inoculum. J Infect Dis 129:45–52

Codeço CT (2001) Endemic and epidemic dynamics of cholera: the role of the aquatic reservoir. BMC Infect Dis 1:1

Colwell RR, Brayton P, Herrington D, Tall B, Huq A, Levine MM (1996) Viable but non-culturable *Vibrio cholerae* O1 revert to a cultivable state in the human intestine. World J Microbiol Biotechnol 12:28–31

Davis W (2012) Unpublished Master's thesis. University of Alberta, pp 49–95

Emch M, Feldacker C, Islam MS, Ali M (2008) Seasonality of cholera from 1974 to 2005: a review of global patterns. Int J Health Geogr 7:31

Faruque SM, INaser B, Islam MJ, Faruque ASG, Ghosh AN (2005) Seasonal epidemics of cholera inversely correlate with the prevalence of environmental cholera phages. PNAS 102:1702–1707

Hartley DM, Morris JG, Jr Smith DL (2006) Hyperinfectivity: a critical element in the ability of *V. cholerae* to cause epidemics. PLoS Med 3:e7

Islam MS, Drasar BS, Sack B (1994) Probable role of blue-green algae in maintaining endemicity and seasonality of cholera in Bangladesh: a hypothesis. J Diarrhoeal Dis Res 12:245–256

Jensen MA, Faruque SM, Mekalanos JJ, Levin BR (2006) Modeling the role of bacteriophage in the control of cholera outbreaks. PNAS 103:4652–4657

Joh RI, Wang H, Weiss H, Weitz JS (2009) Dynamics of Indirectly Transmitted Infectious Diseases with Immunological Threshold. Bull Math Bio. 71:845–862

McCluskey CC, van den Driessche P (2004) Global analysis of two tuberculosis models. J Dyn Diff Equ 16:139–166

Mukandavire Z, Liao S, Wang J, Gaff H, Smith DL, Jr Morris JG (2011) Estimating the reproductive numbers for the 2008–2009 cholera outbreaks in Zimbabwe. PNAS 108:8767–8772

Murphy KM, Travers P, Walport M (2007) Janeways immunobiology, Seventh ed. Garland Science, New York

Pasricha CL, de Monte AJH, OFlynn EG (1936) Bacteriophage in the treatment of cholera. Ind Med Gaz 71:61–68

Singleton FL, Atwell RW, Jangi MS, Colwell RR (1982) Effects of temperature and salinity on *Vibrio cholerae* growth. Appl Environ Microbiol 44:1047–1058

Snow J (1985) On the mode of communication of cholera. John Churchill, London

Tian JP, Wang J (2011) Global stability for cholera epidemic models. Math Biosci 232:31–41